Reliability analysis of battery energy storage system for various stationary applications

Bakeer, Abualkasim; Chub, Andrii; Shen, Yanfeng; Sangwongwanich, Ariya

Published in:
Journal of Energy Storage

DOI (link to publication from Publisher):
10.1016/j.est.2022.104217

Publication date:
2022

Document Version
Accepted author manuscript, peer reviewed version

Reliability Analysis of Battery Energy Storage System for Various Stationary Applications

Abualkasim Bakeer, *Student Member, IEEE,* Andrii Chub, *Senior Member, IEEE,* Yanfeng Shen, *Member, IEEE,* and Ariya Sangwongwanich, *Member, IEEE*

***Abstract*—This paper provides a comparative study of the battery energy storage system (BESS) reliability considering the wear-out and random failure mechanisms in the power electronic converter long with the calendar and cycling aging of the batteries. Three typical stationary applications were considered: frequency containment reserve (FCR), increased self-consumption (ISC) in the case of residential photovoltaic (PV) applications, and peak shaving (PS) in the industrial sector. The mission profile of these applications (e.g., the BESS state-of-charge (SOC) and power) is much different, resulting in the different distribution in the accumulated damage of power electronics components. The random failure analysis based on the MIL-HDBK-217 and wear-out failure rates is carried out for the component and converter levels in each operating regime using the mathematical models. The analysis results revealed that the most prone component in the BESS converter is the dc-link capacitor, where the B_{10} lifetime of the BESS converter is 24, 13, and 15 years for the FCR, ISC, and PS applications, respectively. Moreover, the results show that the capacity fading in the PS applications is much higher than that of the FCR and ISC. In contrast, the capacity fading due to the cycling effect in both the FCR and ISC is dominant.**

***Index Terms*—Battery energy storage system (BESS), degradation, frequency containment reserve (FCR), lifetime, Monte Carlo simulation (MCS), photovoltaic (PV), reliability analysis, stationary applications.**

I. Introduction

BATTERY energy storage systems (BESS) are expected to play an important role in the future power grid, which will be dominated by distributed energy resources (DER) based on renewable energy [1]. Since 2020, the global installed capacity of BESS has reached 5 GWh [2], and an increasing number of installations is predicted in the near future. For instance, more than 50 % of the newly installed residential-scale PV systems in Germany are coupled with BESS [3].

The integration of BESS in stationary applications can alleviate stability and reliability issues in power systems induced by variability in power generation from renewable energy such as wind and photovoltaic (PV) systems. For instance, in large-scale systems (MW range), BESSs have been employed for frequency regulation and grid stabilization [4]-[5]. For a smaller scale such as residential applications, BESSs have been used for increasing self-consumption and peak-shaving in PV applications [6]-[8].

It is essential to ensure the cost-competitiveness of the BESS over its life-cycle. In that respect, the reliability and lifetime of power converters and batteries play an important role in the economic profitability of the BESS when being applied to real applications. It has been demonstrated in [9], [10] that a frequent replacement of power converters and battery packs can increase the system cost significantly, and thus decrease the return of investment significantly in the PV-BESS application. It is thus important to ensure the reliable performance of both power converters and batteries in real operation, e.g., considering mission profiles, where the lifetime modeling approach of both components is needed.

To model the lifetime of the components, the failure mechanisms expected in the real-field operation of the BESS, which consists of both power converters and battery packs, need to be understood. For power converters, power devices and capacitors are known as reliability-critical components, and they have gained much attention in terms of design for reliability [11]-[13]. In general, the wear-out-related failures of the power devices are associated with the interconnection, e.g., bond wire lift-off and solder delamination, where the temperature cycling is one of the main stress factors that accelerate the degradation process [14]. On the other hand, the degradation of the electrolytic capacitor is more related to the chemical reaction, e.g., loss of electrolyte, which results in the loss of capacitance and an increase in the equivalent series resistance (ESR). In this case, the high stored temperature inside the capacitor, referred to as core temperature, is the main factor that increases the degradation rate [15]. Therefore, the lifetime model of both components usually includes these thermal stress factors, and the thermal modeling method also plays an important part in the reliability analysis process.

Lifetime modeling of batteries is typically done by considering the two dominant degradation mechanisms, which are cycling and calendar aging [16]-[18]. The former is mainly induced by the cycling of the state-of-charge (SOC)

This research was supported in part by the Estonian Research Council grant PRG1086, and in part by the Estonian Centre of Excellence in Zero Energy and Resource Efficient Smart Buildings and Districts, ZEBE, grant 2014-2020.4.01.15-0016 funded by the European Regional Development Fund.

A. Bakeer is with the Department of Electrical Engineering, Faculty of Engineering, Aswan University, 81542 Aswan, Egypt, and also with the Power Electronics Group, Department of Electrical Power Engineering and Mechatronics, Tallinn University of Technology, Tallinn 19086, Estonia, (e-mail: abualkasim.bakeer@aswu.edu.eg).

A. Chub is with the Power Electronics Group, Department of Electrical Power Engineering and Mechatronics, Tallinn University of Technology, Tallinn 19086, Estonia (e-mail: andrii.chub@taltech.ee).

Y. Shen is with Danfoss Silicon Power R&D Munich, 85737 Ismaning, Germany. He is also with the Power Electronics Group, Department of Electrical Power Engineering and Mechatronics, Tallinn University of Technology, Tallinn 19086, Estonia (e-mail: yanfeng.shen@taltech.ee).

A. Sangwongwanich is with the Department of Energy Technology, Aalborg University, Aalborg Ø 9220, Denmark (e-mail: ars@et.aau.dk).

during the battery operation, while the latter is related to the standby operation of the battery where the average SOC level is the key parameter (together with other influential factors such as temperature). In this case, the dynamic SOC profile during battery operation for a certain loading condition/profile needs to be obtained from the battery dynamic model, and then applied to the lifetime model of the battery.

In the previous research, the reliability of power converters and battery systems in BESS are usually considered separately. However, there is a potential interaction between the two components in terms of reliability. For instance, the operation of the BESS, e.g., charging/discharging, can affect the loading and thus the reliability of the power converters, as demonstrated in [19]. On the other hand, the energy management strategy, which is usually achieved through the power converter control, dictates the dynamics of the SOC of the battery and thus their degradation rate. Recently, a framework to unify the reliability of power converters and batteries has been developed in [20]. However, it is only applicable for a specific application, e.g., PV self-consumption, which cannot be generally applied to other BESS applications such as frequency regulation, peak-shaving, etc. Thus, a generalized approach to unify the reliability of BESS is still missing.

In this paper, a reliability approach that can be applied to investigate the reliability of BESS in various applications is proposed. The study is performed by normalizing mission profiles of the corresponding applications for their study in the same BESS. An important feature of this study is that it is based on not well-known but publically available high-resolution yearly mission profiles measured in real BESSs. This provides a rare possibility to reproduce the given study, enhance the proposed methodology, or perform a cost-related study including the lifecycle cost of BESS. Section II describes the case study power electronic converter as well as application-specific mission profiles used in the further study. Section III introduces the proposed methodology for wear-out and random failure analysis of the power electronic converter along with the results of accumulated damage calculations and consequent Monte-Carlo simulations at the components level. Section IV summarizes the system-level reliability of the power electronic converter (PEC) and estimated degradation of the BESS. Based on these, conclusions are drawn in Section V.

II. Description of the Studied System and Application Specific Mission Profiles

A. Power Electronics Converter

This study employs a conventional PEC that consists of two conventional power stages: a bidirectional buck/boost dc-dc converter coupled with a grid-tied three-phase two-level voltage source inverter (VSI). Dc-link capacitor C_1 smoothes out intermediate dc voltage between the two stages. The input inductor L_{in} ensures the low-ripple current of the BESS with the operating voltage of V_{ESS}. The PEC utilizes eight discrete IGBTs of the same type from Infneon's TrenchStop® Series, which suits the rated power of 10 kW. For simplicity, L-filters were used for the grid current filtering at the switching frequency of 10 kHz. The key parameters of the case study PEC are summarized in Table I.

The control system presented in Fig. 1 is based on conventional algorithms. In particular, a typical dual-loop control is applied to the dc-dc stage, where the internal loop regulated the current of the input inductor, while the outer loop regulated the dc-link voltage V_{dc}. The input voltage of the dc-dc stage will vary with the SOC of the BESS. However, the battery stack should never provide voltage higher than the dc-link voltage, even at the SOC level of 100%. This is easily ensured by the stack design, while the battery voltage range depends on the battery type. This study considers Lithium-Ion batteries.

The control of the grid-side VSI is decoupled from the control of the dc-dc stage. VSI control system utilizes a phase lock loop providing the grid angle θ based on the measured grid voltages. It is used to implement the grid current control in the rotating reference frame utilizing conventional proportional-integral (PI) controllers. The mission power profile corresponding to a certain application defines the active power delivered/drawn from the point of common coupling (PCC). The reference reactive power is set to zero in this study, while it can be used to provide ancillary services depending on the application. This study is focused on the active power only, as the available yearly mission profile datasets (described in the next subsection) do not consider the reactive power. Future studies can be extended to analyze the effect of the reactive power on PEC reliability. However, it could be predicted that the most significant influence will be observed in the thermal cycling of the semiconductor components.

The used control system is typical in both academic research and industry. The given PEC was implemented in the PLECS software with loss/thermal models of the main components to extract values and construct look-up tables of the current stresses, thermal cycles, etc.

B. Application-Specific Yearly Mission Profiles

BESSs are becoming a ubiquitous part of modern and future power systems. Their use spans over a wide variety of applications, from utility to residential applications [21]-[22].

This study takes advantage of the recently published open data results of the study [23]. Based on the known yearly profiles of the distribution grid frequency, energy generation and consumption in a household with a PV system, and clustering of industrial loads, that study provides six high-resolution mission profiles in three main groups. Each profile contains power and SOC information among others. One profile from each of the three presented groups is employed in this study.

TABLE I. Parameters of the Two-Stage Converter Used in the Study.

Parameter	Value/Part Number
Switching frequency (F_{SW})	10 kHz
Buck-boost inductor (L_{in})	5 mH
IGBT discrete switch with antiparallel diode	IKW25T120
Dc-link capacitor (C_1)	470 µF
Dc-link voltage (V_{dc})	700 V
Grid current filter (L_f)	5 mH
RMS grid voltage (RMS L-L) (V_g)	380 V
Grid frequency (f)	50 Hz

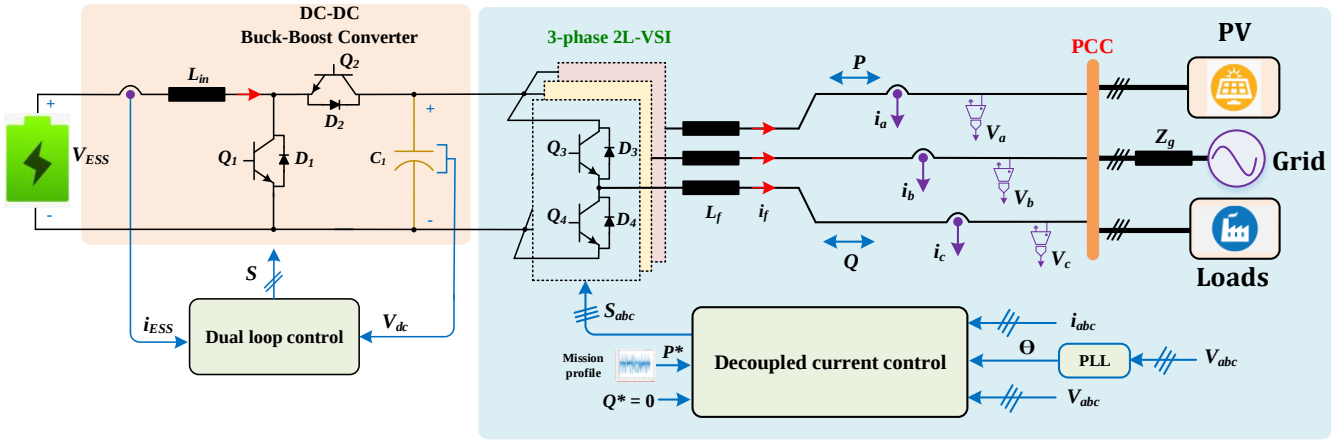

Fig. 1. Configuration of a 10 kW two-stage PEC for BESS.

Three mission profiles described below were normalized to the same peak power of 10 kW to make them compatible with the case study system and provide a holistic analysis demonstrating key differences in how these profiles influence the reliability of the BESS system with PEC.

1. *Frequency Containment Reserve (FCR) for Utility-Scale Applications*

The most common application of BESSs in the utility grids is related to frequency stabilization in view of the proliferation of renewable energy sources providing intermittent power with low inertia. Fig. 2*a* shows the yearly power profile of the FCR applications after normalization to the power rating of the given PEC. It also includes a two-day zoomed plot from June to demonstrate that the FCR power profile is highly variable bit mostly within the range of ±5 kW. This behavior is typical for the FCR applications, where the peak power is used only during rare critical grid frequency deviations. Another typical feature of the FCR applications is SOC management to keep it at the average level of 50%, as shown in Fig. 2*b* for one-year and two-day scales. This allows for providing lower aging of batteries along with good availability of the FCR service. These features distinguish FCR applications from others described below.

2. *Increased Self-Consumption (ISC) in Residental PV+BESS Setting with Greedy Algorithm*

In residential applications, different energy management algorithms could be used. The yearly power profile demonstrated in Fig. 3*a* corresponds to the greedy algorithm that stores surplus energy from PV in the BESS (until SOC of 100%) and compensates for the difference when PV does not supply enough power. This algorithm provides maximum power cycling in residential applications and thus makes for an excellent opportunity for the worst-case reliability analysis. Consequently, the SOC of the battery is changing in a wide range, as shown in Fig. 3*b*, providing the maximum cycling aging in residential applications. Also, this power management algorithm provides the most variety in frequency and charge/discharge rates compared to algorithms based on feed-in damping [23]. Also, it is much different from the FCR application, facilitating the targets of this study.

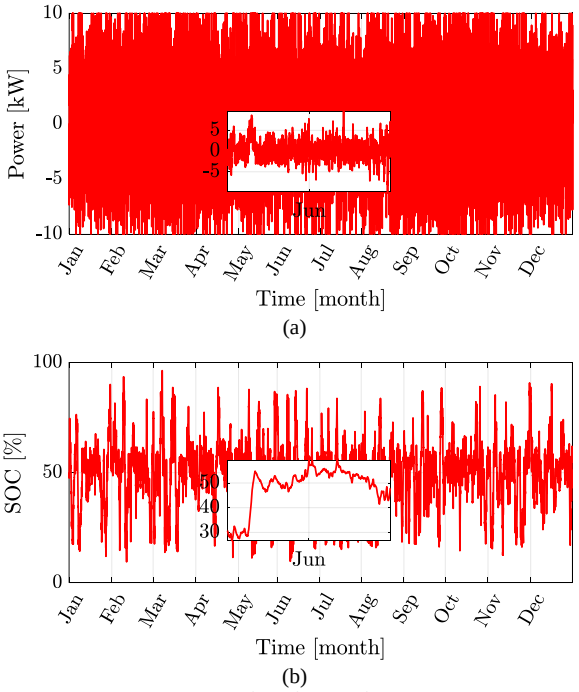

Fig. 2. Yearly mission profile of BESS for FCR applications [23]: (a) converter power, and (b) SOC.

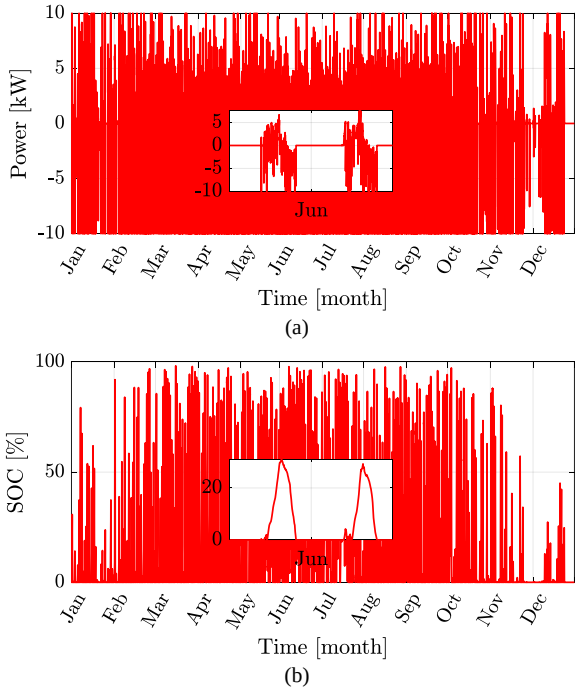

Fig. 3. Yearly mission profile of BESS for ISC applications [23]: (a) converter power, and (b) SOC.

3. *Peak Shaving (PS) Storage System for Industrial Applications*

The third power profile selected for this application corresponds to peak shaving applications in the industry. As could be appreciated from Fig. 4*a*, the BESS provides energy mostly during the summer months. This profile corresponds to a cluster of industrial consumers with an average load of 70-80% of power line capacity during the day and 20-30% during the night. Moreover, the considered cluster draws the typical mightly basic load during weekends. BESS takes over any load over a certain threshold, which happens rarely. This results in the fewest number of charge/discharge cycles of the battery. The distinguishing feature of this application is in SOC management at 100% during idle periods, which aims to improve the availability of the PS service. Based on the SOC profile from Fig. 4*b*, it could be predicted that this application should cause the highest calendar aging of the battery. Considering the high requirements to the availability of the PS services, in the study, PEC is considered always connected online and operating at zero power reference. This, however, will have a minor influence on the wear-out of the semiconductors as temperature cycling at zero power is negligible.

III. Electro-Thermal and Lifetime Modeling of Power Electronics Component

A. *Methodology*

Based on the classical life cycle bathtub curve, there are three regions for electronics devices over time, i.e., early infant mortality failure, constant random failure, and wear-out failure as shown in Fig. 5. The early life failures can be addressed using techniques such as burn-in or various screening tests. The random failure of components plays an important role in system failure probability, particularly at the early stage of the useful life. As the service time increases, the wear-out of components dominates the failure probability.

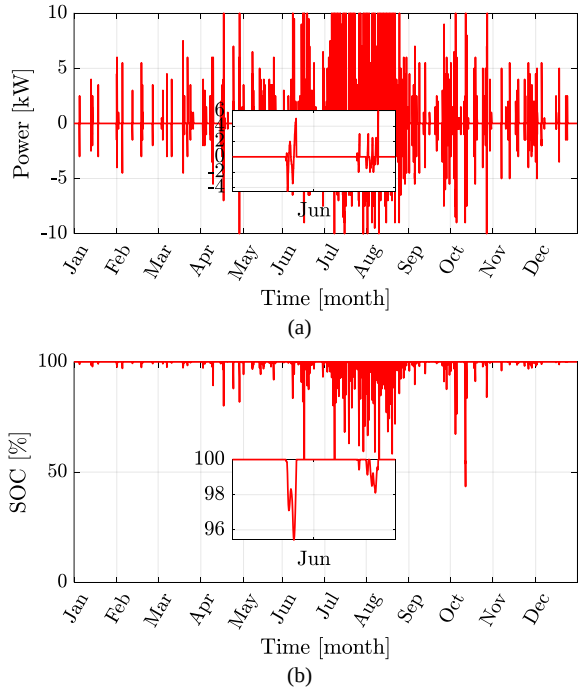

Fig. 4. Yearly mission profile of BESS for PS application [23]: (a) converter power, and (b) SOC.

This article takes into account both the random failure and the wear-out failure, comprehensively evaluating the system failure probability of the energy storage system. Taking into account both the wear-out and random failure rates, a systematic failure evaluation method is proposed, as shown in Fig. 6. It is reported in [11] that power cycling is the most critical stress factor determining the failure of power electronics converters; therefore, accurate electro-thermal modeling is included in Fig. 6.

A real-field mission profile of the energy storage system (power and SOC with respect to time, shown in Section II-B) is the input of the reliability analysis flowchart. With detailed electrical models of components, the mission profile is translated into time-domain power loss profiles, which are further converted to the junction/hotspot temperature profiles with the thermal models of components. It is noted that the power losses of components are temperature-dependent. Therefore, the derivation of junction/hotspot temperature is iterative. The wear-out of capacitors is mainly caused by the real-time hotspot temperature, whereas that of power semiconductor devices is attributed to temperature fluctuations. To quantify the degradation of power semiconductor devices, their temperature profiles need to be processed with the rainflow counting algorithm, extracting the number of cycles for different combinations of temperature swing, mean junction temperature, and heat-on time. These temperature cycles can be translated into static damages with lifetime models of power semiconductor devices. For capacitors, their hotspot temperature can be directly converted to static damages with their lifetime models. In practice, however, the parameters of both semiconductor devices and capacitors vary over certain ranges. Considering the parameter variations, we can perform a Monte Carlo simulation on the accumulated damage of components, yielding the failure probability density functions over time for different components.

Combining the wear-out and random failure rates, we can obtain the equivalent failure rates for different components. The series model is then used to transform the failure rates of individual components into the failure rate of the converter, assuming the converter fails when the first component fails and all components fail or survive independently with each other. Finally, the degradation of battery cell capacity caused by storage conditions and power cycling is taken into account, leading to the lifetimes of BESS for various stationary applications.

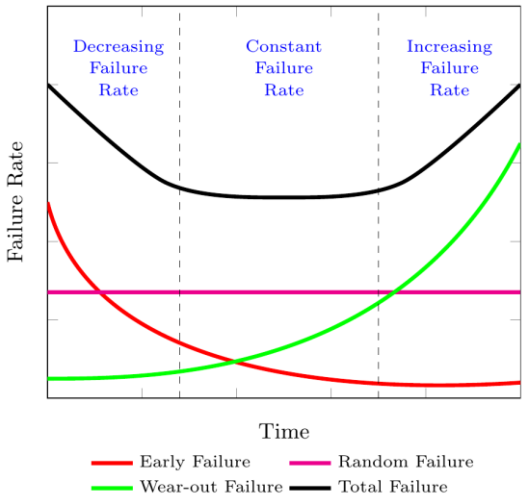

Fig. 5. Typical lifecycle bathtub curve.

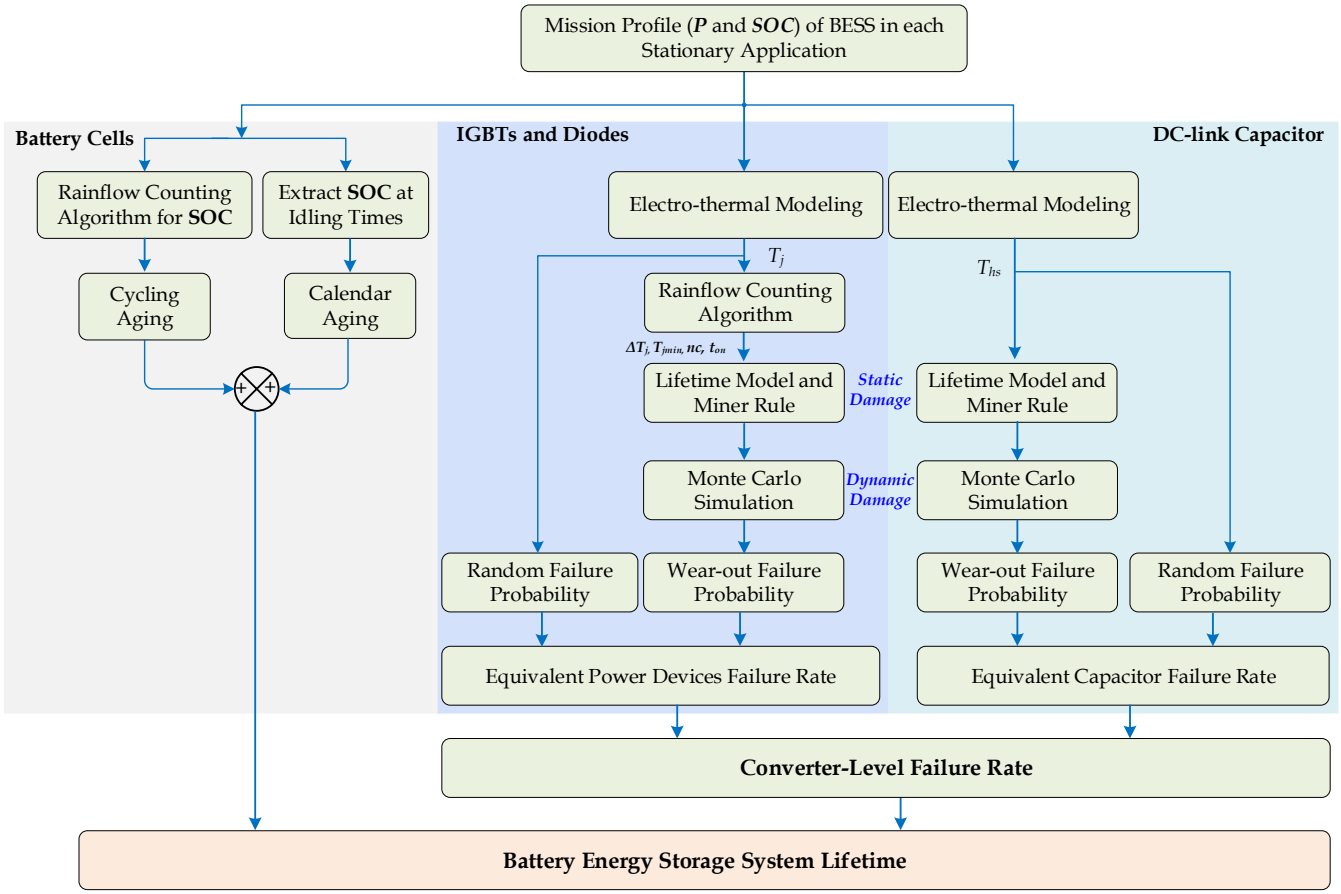

Fig. 6. Methodology of the reliability analysis for the BESS converter in the case study.

B. *Electro-thermal Modeling*

1. *DC-link Capacitor*

A practical capacitor can be modeled as an ideal capacitor in series with an equivalent series resistor (ESR) when the frequency is not extremely high. Aluminum electrolytic capacitors can be a good choice for the implementation of dc-link due to their higher energy density and lower cost compared with film and ceramic capacitors. Generally, there are two wear-out mechanisms in electrolytic capacitors: 1) chemical reactions due to electrolyte evaporation and contaminants, leading to the deterioration of the dielectric material, and 2) localized heating, ion transport, and chemical processes caused by the leakage current. The main stressor is the internal hotspot temperature, which is determined by the power loss and the thermal resistance [24]. The power loss can be calculated with

$$P_{loss,C_1} = \sum_i I_{C_1,rms}^2(f_i)\ \ ESR(T_{hs}, f_i) \tag{1}$$

where $I_{C1,rms}(f_i)$ represents the rms of the current ripple harmonic at the frequency f_i, T_{hs} denotes the hotspot temperature of the capacitor. It is noted that the *ESR* is both temperature- and frequency-dependent.

As seen in Fig. 1, the dc-link capacitor is interfaced with both a dc-dc converter and a three-phase inverter. Therefore, the dc-link capacitor needs to absorb the current ripples from both converters. The ripple current flowing through the dc-link capacitor is determined by the operating conditions of both the dc-dc converter and the inverter, e.g., power, duty cycle, switching frequency, modulation index, power factor, and temperature [25]. The calculation of the real-time power loss can be tedious and time-consuming. Therefore, this work uses look-up tables to obtain the real-time power loss of the dc-link capacitor. The ESR dependency on T_{hs} and f_i is extracted from the datasheet of the ESMM451VSN471MA45S capacitor [26] and is then modeled in PLECS. The dc-link capacitor bank (C_1 in Fig.1) consists of four capacitors: two of which are connected in parallel to handle the ripple current, and two in series to match the voltage stress. Then the power loss of the dc-link capacitor bank is simulated in PLECS for different combinations of operating conditions and different applications, generating a look-up table. Fig. 7 shows typical power losses of the dc-link capacitor at different BESS stationary applications in the case study.

The hotspot-ambient thermal resistance of an aluminium electrolytic capacitor can be calculated as [27]:

$$R_{th,ha} = \frac{4}{\alpha\beta\pi D(D+4H)} \tag{2}$$

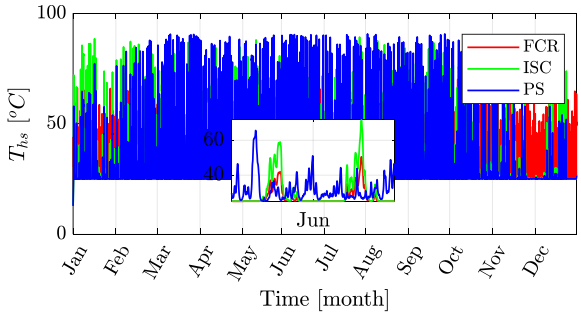

Fig. 7. Estimated yearly hot-spot temperature of the dc-link capacitors for different BESS applications.

where α denotes the temperature rise ratio, β represents the heat radiation constant, D is the capacitor diameter, and H denotes the capacitor height. The hotspot temperature T_{hs} can be calculated as

$$T_{hs} = T_a + R_{th,ha} \; P_{loss,C_1} \tag{3}$$

where T_a represents the local ambient temperature of the dc-link capacitor.

2. Power Semiconductor Devices (IGBTs and Diodes)

The power loss of IGBTs consists of the conduction losses and switching losses (turn-on and turn-off losses). Both the conduction and switching losses change concerning the battery voltage and the operating power, and they are temperature-dependent. On the other hand, the junction temperature is determined by the power loss with the convolution of the junction-ambient thermal impedance. The mutual dependency of power loss and junction temperature complicates the derivation of accurate junction temperature when real-field mission profiles are applied.

To simplify the calculation process of power losses of semiconductor devices with a long-term mission profile, the power loss model and thermal model of the used IGBTs are developed in PLECS software. Meanwhile, the heatsink of the IGBTs is also included in PLECS simulations. Thus, we can obtain the power losses and junction temperatures of IGBTs under different operating conditions (i.e., different T_a and P). A detailed power and junction temperature look-up table (LUT) can be created for the fast temperature prediction when different mission profiles are applied. The simulated power losses of IGBTs in the Buck-Boost converter and the 2L-VSI for different BESS applications are shown in Fig. 8.

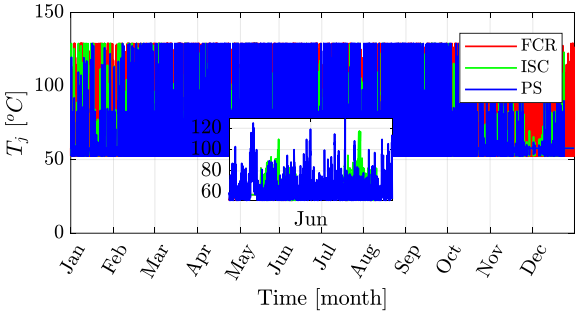

Fig. 8. Junction temperature of the 2L-VSI IGBT at different BESS stationary applications.

C. Lifetime Modeling

1. DC-link Capacitor

A widely used capacitor lifetime model is employed for the lifespan projection of capacitors [28]

$$L_t = L_0 \, 2^{\frac{T_0 - T_{hs}}{n_1}} \left(\frac{V_t}{V_0}\right)^{-n_2} \tag{4}$$

where L_0 is the nominal lifetime in the datasheet, T_0 is the nominal capacitor temperature, V_t is the applied voltage, and V_0 is the rated voltage given in the datasheet.

Based on the commonly-used Miner's rule, the damage is assumed to be accumulated linearly, as

$$AD = \sum_{i=1}^{k} \frac{\Delta t}{L_k} \tag{5}$$

where k is the mission profile length, Δt is the sampling interval of the mission profile in seconds, and L_i denotes the lifetime of the ith interval with a hotspot temperature $T_{hs,I}$, and a voltage $V_{t,i}$.

As the accumulative damage increases, the lifetime L_t in (4) becomes shorter. Accordingly, the wear-out of the capacitor is accelerating over time as ESR increases with the damage. Considering the feedback of degradation level (i.e., ESR damage-caused drift) on the lifetime model, the accumulated damage curves for different applications are shown in Fig. 9.

2. Power Semiconductor Devices (IGBTs and Diodes)

Various empirical lifetime models based on a statistical analysis of available accelerated lifetime testing data can be found in the literature. The temperature of studied system components varies during its loading, which affects the mechanical lifetime fatigue model. Also, the importance of considering the dependency between the heating time and the temperature cycle has become outstanding. This leads to employing the Coffin-Manson-Arrhenius lifetime model [29]-[30]. In this paper, the empirical lifetime model for IGBT 4 [31] is used

$$N_f = A\Delta T_j^{\alpha} \exp\left(\frac{\beta}{T_{j\min}}\right)\left(\frac{t_{on}}{1.5}\right)^{-0.3} ; \quad 0.1s \le t_{on} \le 60s \tag{6}$$

where ΔT_j denotes the thermal cycle amplitude in ^oC, T_{jmin} is the minimum junction temperature during the thermal cycle in ^oC, t_{on} is the heating time in second, and α, β are the curve fitting parameters.

It is also assumed that the damage of IGBT accumulates linearly, as

$$AD = \sum_{i=1}^{N} \frac{n_{f,i}}{N_{f,i}} \tag{7}$$

where N stands for the total number of power cycles generated by the rainflow counting algorithm, $n_{f,i}$ is the number of cycles for i^{th} power cycle (i.e., either 1 or 0.5), $N_{f,i}$ is the number of cycles to failure at the corresponding ΔT_j and T_{jmin} in the i^{th} power cycle.

The annual accumulated damages of components for different applications are shown in Fig. 10. Compared with power semiconductor devices, the dc-link capacitor always has higher damage than other components.

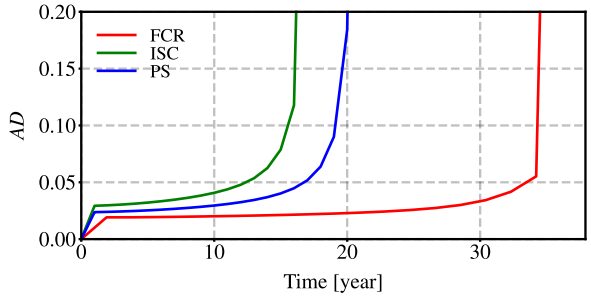

Fig. 9. Damage feedback of the dc-link capacitor considering the degradation level and hot spot temperature effects on the capacitor ESR.

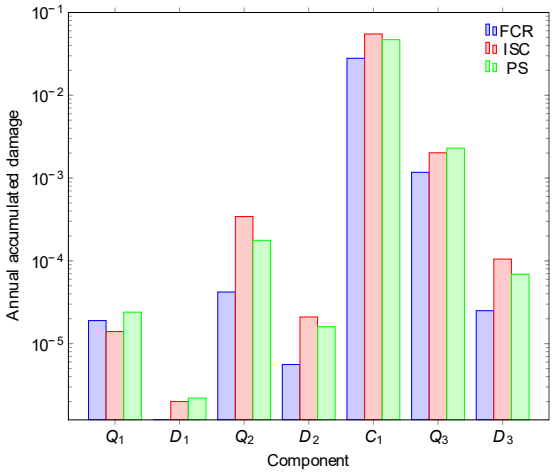

Fig. 10. Visualization of the static damage for each component in the three stationary applications.

TABLE II. STATIC VALUES OF THE LIFETIME ANALYSIS OF THE CONVERTER POWER DEVICES

Term	Q_1			D_1			Q_2			D_2			Q_3			D_3		
	FCR	ISC	PS	FCR	ISC	PS	FCR	ISC	PS	FCR	ISC	PS	FCR	ISC	PS	FCR	ISC	PS
ΔT_j (°C)	16.79	15.38	16.7	9.26	10.2	10.1	20.1	30.8	26	13.1	16.8	15.5	16.8	15.6	15.9	14.5	14.4	14.2
	-	-	-	-	-	-	-	-	-	-	-	-	13.9	15.6	16.3	5.29	8.02	7.17
T_{jmin} (°C)	47.34	48.68	50.10	39.75	43.1	42.3	47.8	58.3	53	41.27	47.6	45.4	60.8	62.6	63.7	53.9	57.0	56.9
	-	-	-	-	-	-	-	-	-	-	-	-	60.8	62.6	63.7	53.9	57.0	56.9
$nc \times 10^6$	2.08	2.46	3.10	0.83	2.46	3.1	2.12	2.46	3.1	2.16	2.46	3.09	2.08	2.46	3.10	2.31	2.4	3.09
	-	-	-	-	-	-	-	-	-	-	-	-	1.57×10^3					
$N_f \times 10^9$	110.3	170.2	127.3	1795	1146	1380	49.7	7.18	17	361.1	116	189	88.2	126	122	187	194	221
	-	-	-	-	-	-	-	-	-	-	-	-	1373	787	694	109513	16883	28688
t_{on} (sec)	59.05	47.30	34.90	52.57	43.7	31.1	67.2	40.4	36	60.60	46.8	36.5	74.8	53.1	42.3	72.9	52.6	42.1
	-	-	-	-	-	-	-	-	-	-	-	-	0.01					
Annual *AD* $\times 10^{-4}$	0.19	0.14	0.24	0.012	0.02	0.02	0.42	3.43	1.8	0.056	0.21	0.16	0.24	0.19	0.25	0.11	0.12	0.14
	-	-	-	-	-	-	-	-	-	-	-	-	11.5	20.0	22.7	0.14	0.93	0.55
	0.19	0.14	0.24	0.012	0.02	0.02	0.42	3.43	1.8	0.056	0.21	0.16	11.7	20.2	22.9	0.25	1.0	0.69
Lifetime (year) $\times 10^2$	528.7	689.7	410.6	8302	4655	4455	233	29.1	56	1672	474	612	423	514	395	877	790	716
	-	-	-	-	-	-	-	-	-	-	-	-	8.71	4.99	4.40	694	107	182
	528.7	689.7	410.6	8302	4655	4455	233	29.1	56	1672	474	612	8.54	4.95	4.36	400	100	144.9

Color code: Long-cycle, Short-cycle, Total

D. Monte-Carlo Simulation and Weibull Distribution Function

With the static annual wear-out damage obtained, a Monte Carlo simulation is conducted considering 20% variations in the parameters (ESR = 0.56 Ω, L_0 = 3000 hours, T_0 = 85 °C, V_0 = 450 V, n_1 = 10, n_2 = 5) related to the capacitor and the parameters of (A=9.34×10^{14}, α=4.416, β=1285, ΔT_j, T_{jmin}, nc, t_{on}) related to the IGBT. The results obtained from the static damage analysis are given in Table II.

The Monte Carlo simulation results for the dc-link capacitor and inverter IGBT under different application mission profiles are shown in Fig. 11. It is seen that the probability density of the wear-out failure of each component varies over the operation time. The corresponding wear-out failure probability of each critical component can be obtained by integrating the pdf with respect to time.

To facilitate the system failure analysis, the *probability density (pdf)* curves in Fig. 11 are fitted with the Weibull distribution. The scale parameter α and the shape parameter β for critical components are listed in Table III.

TABLE III. WEIBULL PARAMETERS OF EACH COMPONENT IN THE DIFFERENT APPLICATIONS IN THE CASE STUDY.

Component	FCR		ISC		PS	
	α	β	α	β	α	β
Q_1	35888.58	4.28	46745.04	4.53	28040.39	4.35
D_1	**536110.71**	5.18	**306026.08**	5.01	**291014.92**	5.10
Q_2	15976.91	4.14	2098.24	3.70	3950.71	3.88
D_2	109952.87	4.64	32045.18	4.31	40992.14	4.40
C_1	**38.42**	5.86	**19.56**	5.83	**23.13**	5.89
Q_3	608.43	4.58	359.74	4.45	300.67	4.43
D_3	26304.10	5.70	6474.91	5.41	9569.22	5.60

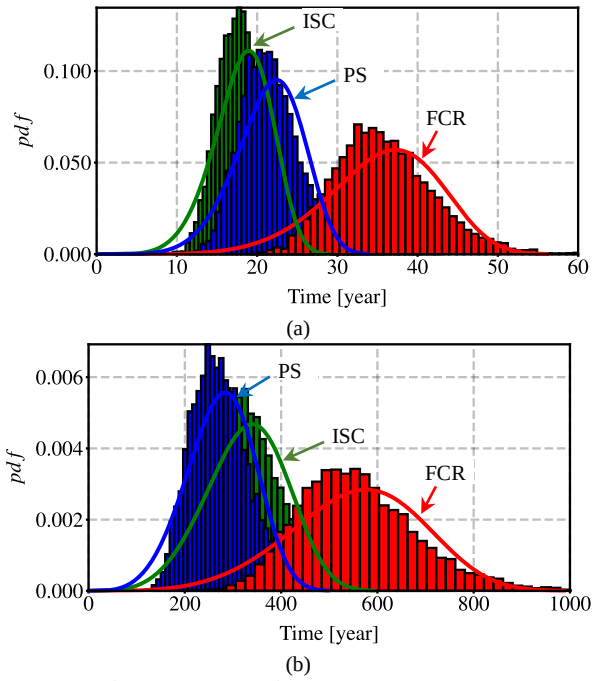

Fig. 11. Lifetime distribution for the key converter components in the studied PEC for various applications: (a) dc-link capacitor and (b) inverter IGBT.

IV. System-Level Reliability

A. PE-Converter Reliability

Apart from mission-profile-related damage, the random failure rate of components should be considered. It could be calculated using either MIL-HDBK-217F [32]-[33] or FIDES [34] handbook. The latter considers the influence of the mission profile on the random failure rates and, thus, suits applications where a converter operates outdoor the most, like photovoltaic power systems [34]. The MIL-HDBK-217F handbook provides the most conservative estimate and, therefore, is still popular in the design of mission-critical systems.

This study considers the constant ambient temperature of 25°C, since a BESS typically operates in an air-conditioned environment to minimize hazards associated with the usage of Lithium-based batteries. Consequently, the considered BESS mission profile is independent of weather conditions. Therefore, this study utilizes the approach based on the MIL-HDBK-217F handbook for simplicity. The annual rates are provided in Table IV. It has a steady failure rate throughout time. While the wear-out failure rate of each component can be extracted from the Weibull parameters as a function of the time as

TABLE IV. Annual Random Failure Rate for Each Component of the Converter in Different Applications

Component	FCR	ISC	PS
Q_1	0.0001456	0.0001523	0.0001446
D_1	**0.0000394**	**0.0000413**	**0.0000389**
Q_2	0.0001470	0.0001532	0.0001476
D_2	0.0000416	0.0000447	0.0004131
C_1	**0.0011550**	**0.0011550**	**0.0011550**
Q_3	0.0001902	0.0002006	0.0018912
D_3	0.0000610	0.0000659	0.0000600

$$\lambda(t) = \beta\left(\frac{1}{\alpha}\right)^{\beta} t^{(\beta-1)} \tag{8}$$

where α and β are the scale and shape parameters of Weibull fitting, respectively; while t is the time in years.

The failure rate of the BESS PEC in each application is plotted in Fig. 12. The total unreliability function of the PE part in the studied system can be derived as

$$F_{con}(x) = 1 - \prod_{j=1}^{comp} (1 - F_j(x)) \tag{9}$$

in which $F_j(x)$ is the unreliability function of j^{th} component in the converter.

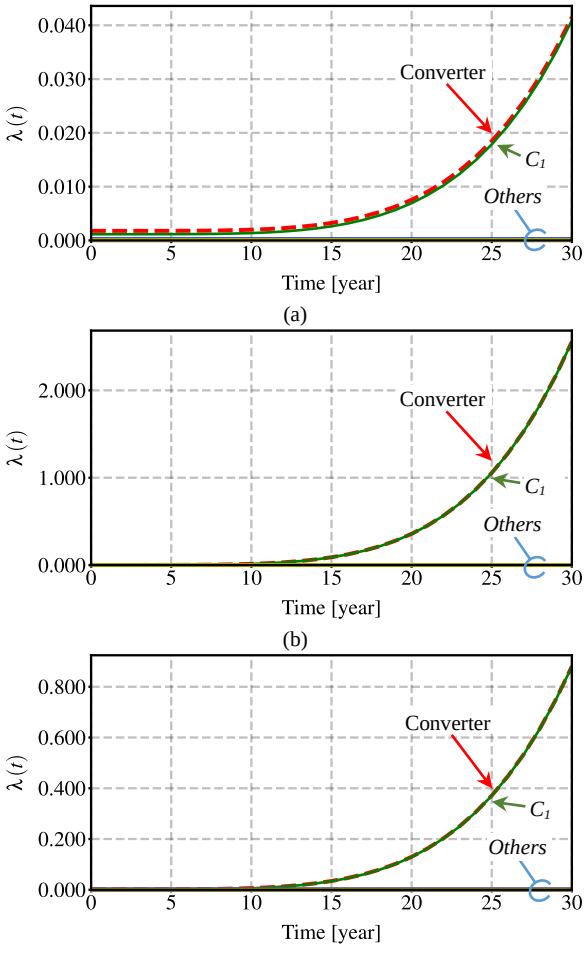

Fig. 12. The failure rate of BESS converter for various applications: (a) FCR, (b) ISC, and (C) PS.

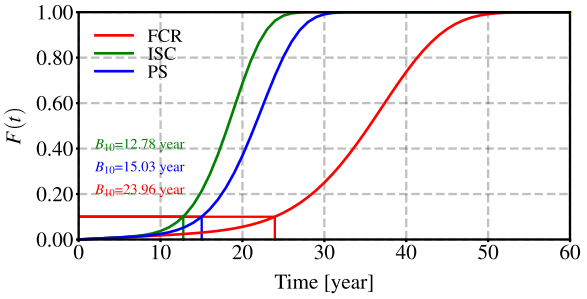

Fig. 13. BESS converter reliability for various applications.

B. *Degradation of BESS*

When utilizing the BESS for a variety of purposes, one of the most challenging issues is battery lifetime, since the capacity of the battery should not decline rapidly within a short period of operation. Also, the battery lifetime impacts economic evaluation from another perspective. Generally, the main source of degradation in the battery lifetime include the idling and cycling operation [35]. When the battery doesn't supply power and the SOC remains constant, during these idle intervals the battery loses its capacity due to calendar aging. The capacity fade of the Li-ion battery due to calendar aging ($C_{f,calendar}$) is experimentally investigated and can be expressed as [36]:

$$C_{f,calendar} = 0.1723\, e^{0.007388 SOC_{avg}} t^{0.8} \quad (10)$$

where SOC_{avg} is the average SOC of the battery during storage, t is the storage time (i.e., battery is in the idling mode) expressed in months.

It should be pointed out that the degradation modeling due to the calendar aging in (10) has been derived with the assumption of the Li-ion battery is operating at 25 ^oC by employing air-conditioning systems. Moreover, the idling times are extracted from the SOC profile, which corresponds to the zero intervals in the BESS power profile. Then, the average value is calculated for the obtained times over the whole year.

The capacity fading due to the cycling aging of the battery ($C_{f,cycle}$) is dependent on the number of cycles, average SOC during the cycle, and the cycle swing as in (11). These parameters can be extracted from the SOC mission profile in Section II-B for each BESS application by applying the rainflow counting algorithm [37].

$$C_{f\_cycle} = 0.021 e^{-0.01943\, SOC} cd^{0.7162} nc^{0.5}, \quad (11)$$

where SOC is the average SOC of the power cycle in (%), cd is the cycle depth in (%), and nc is the number of cycles.

The analysis results of the SOC mission profile in Section II-B for the three applications using the rainflow counting algorithm in MATLAB software [38] are given in Fig. 14.

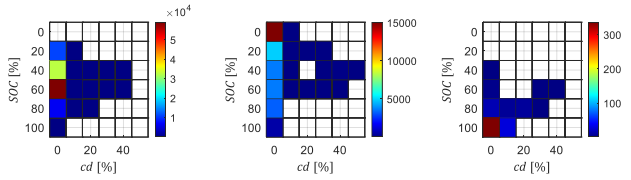

(a) (b) (c)

Fig. 14. 2D plot of the rainflow counting for the BESS SOC at various stationary applications: (a) FCR, (b) ISC, and (c) PS.

The linear damage accumulation rule can be utilized to find the effect of power cycling obtained from the rainflow counting on the battery capacity fading from the cycling aging [39]. Based on Miner's rule and (11), the capacity fading due to cycling as a function of the time can be given as in (12). From (3) and (4), the capacity fade as a function of time can be derived as:

$$C_{f,cycle} = \sqrt{\sum_{j=1}^{K} \left(0.021\, e^{-0.01943 SOC} cd^{0.7162}\right)^2 nc\, t} \quad (12)$$

where K is the number of different depths of discharge and t is the time in the same unit of the SOC mission profile length (i.e., in years during the case study).

The total capacity fade of the battery equals the sum of both calendar and cycle aging as described in the left part of the flowchart given in Fig. 6. The analysis results for the battery degradation in the understudy stationary applications are given in Fig. 15. It can be noted that the capacity fading has a nonlinear profile with the operating time. When we assume that 20% fade is the criteria at which the BESS reaches the end of its useful life, the battery in the ISC application fades the quickest when compared to the FCR and PS applications. Fig. 15c indicates that the capacity fading due to storage is dominant in the PS applications as the BESS exchanges power in a short period over the year, while it stores energy close to 100% SOC.

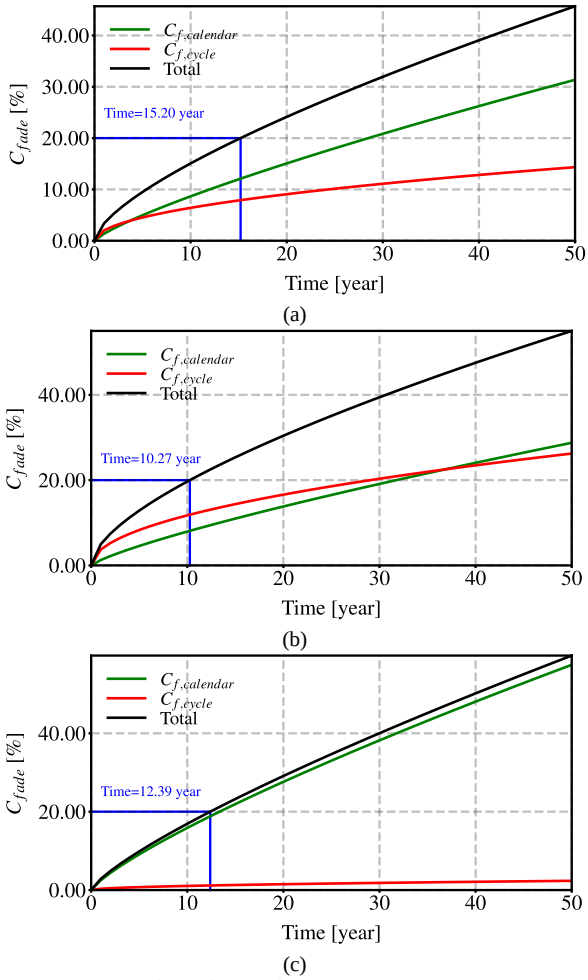

Fig. 15. Capacity fade of BESS for various stationary applications in the study: (a) FCR, (b) ISC, and (C) PS.

V. Conclusions

The paper provides a systematic study of BESS reliability including the associated power electronic converter. Three main groups of applications were considered: utility – frequency containment reserve, residential PV – increased self-consumption with a greedy algorithm, and industrial – peak shaving of excessive load power. The estimations are provided using the same case study system to ensure comparability of the results

Residential applications are proven to be the most challenging as they feature the shortest lifetime of both converter and battery – 13 and 10 years, respectively. It is

worth mentioning that the battery lifetime is defined at the 20% capacity fade, while a 10% failure rate is used for the converter. If one of these criteria is changed, it is possible to match the expected lifetimes, to a reasonable extent.

In the frequency containment reserve applications, the expected lifetime of the power electronic converter of 24 years allows for one replacement of batteries that fade by 20% of their capacity in 15 years. However, if the fade of 30% is allowed, the lifetime of the converter and battery could be matched.

In the peak shaving applications, BESS suffers from the highest calendar aging due to average SOC close to 100%. On the other hand, the low number of charge/discharge cycles allows for a capacity fade of 20% in 12 years. This is close to 15 years of B_{10} lifetime expected from the associated converter.

Considering rapidly growing market prices for energy and ancillary services, in some regions, like Northern Europe, future research could extend the presented results with an economic analysis of lifecycle cost and return of investments.

REFERENCES

[1] K. C. Divya and J. stergaard, “Battery energy storage technology for power systems,” in *Elect. Power Syst. Res.*, vol. 79, pp. 511–520, 2009.

[2] PV magazine, “Strong growth ahead for battery storage” [Online] Available: https://www.pv-magazine.com/2021/04/13/strong-growth-ahead-for-battery-storage/. Accessed on: Jun.18 2021.

[3] A. Rathi, “100 000 homes in Germany now have battery storage systems connected to the grid,” 2018. [Online]. Available: https://qz.com.

[4] T. Thien, D. Schweer, D. vom Stein, A. Moser, and D. U. Sauer, “Real-world operating strategy and sensitivity analysis of frequency containment reserve provision with battery energy storage systems in the German market,” in *Journal of Energy Storage*, vol. 13, pp. 143–163, 2017.

[5] D. I. Stroe, V. Knap, M. Swierczynski, A. I. Stroe, and R. Teodorescu, “Operation of a grid-connected lithium-ion battery energy storage system for primary frequency regulation: A battery lifetime perspective,” in *IEEE Trans. Ind. App.*, vol. 53, no. 1, pp. 430–438, Jan 2017.

[6] SMA Solar Technology AG, “Planning guidelines - the system solution for more independence,” 2013. [Online]. Available: https: //files.sma.de/dl/1353/SI-HoMan-PL-en-51.pdf.

[7] G. Merei, J. Moshövel, D. Magnor, and D. U. Sauer, “Optimization of self-consumption and techno-economic analysis of PV-battery systems in commercial applications,” in *Applied Energy*, vol. 168, pp. 171–178, 2016.

[8] A. Zeh and R. Witzmann, “Operational strategies for battery storage systems in low-voltage distribution grids to limit the feed-in power of roof-mounted solar power systems,” in *Energy Procedia*, vol. 46, pp. 114-123, 2014.

[9] M. Sandelic, A. Sangwongwanich, and F. Blaabjerg, "Impact of Power Converters and Battery Lifetime on Return of Investment of Photovoltaic Systems," in proc. IPEMC2020-ECCE Asia, 2020, pp. 1395-1401.

[10] T. J. Formica, H. A. Khan, and M. G. Pecht, “The effect of inverter failures on the return on investment of solar photovoltaic systems,” in *IEEE Access*, vol. 5, pp. 21336–21343, 2017.

[11] H. Wang, M. Liserre, and F. Blaabjerg, “Toward reliable power electronics: Challenges, design tools, and opportunities,” in *IEEE Ind. Electron. Mag.*, vol. 7, no. 2, pp. 17–26, Jun. 2013.

[12] H. Wang and F. Blaabjerg, “Reliability of capacitors for dc-link applications in power electronic converters - an overview,” in *IEEE Trans. Ind. App.*, vol. 50, no. 5, pp. 3569–3578, Sep. 2014.

[13] S. Yang, A. Bryant, P. Mawby, D. Xiang, L. Ran, and P. Tavner, “An industry-based survey of reliability in power electronic converters,” in *IEEE Trans. Ind. App.*, vol. 47, no. 3, pp. 1441–1451, May 2011.

[14] V. Smet et al., “Ageing and failure modes of IGBT modules in high temperature power cycling,” in *IEEE Trans. Ind. Electron.*, vol. 58, no. 10, pp. 4931–4941, Oct. 2011.

[15] Application guide, Aluminum Electrolytic Capacitors, Cornell Dubilier, Liberty, SC, USA. [Online]. Available: http://www.cde.com/catalogs/AEappGUIDE.pdf

[16] D. Magnor, J. B. Gerschler, M. Ecker, P. Merk, and D. U. Sauer, “Concept of a battery aging model for lithium-ion batteries considering the lifetime dependency on the operation strategy,” in proc. of EU PVSEC, vol. 24, 2009.

[17] D. Stroe, M. Swierczynski, A. Stroe, R. Laerke, P. C. Kjaer, and R. Teodorescu, “Degradation behavior of lithium-ion batteries based on lifetime models and field measured frequency regulation mission profile,” in IEEE *Trans. Ind. App*., vol. 52, no. 6, pp. 5009–5018, Nov. 2016.

[18] G. Angenendt, S. Zurmuhlen, H. Axelsen, and D. U. Sauer, “Comparison ¨ of different operation strategies for PV battery home storage systems including forecast-based operation strategies,” in *Appl. Energy*, vol. 229, pp. 884 – 899, 2018.

[19] A. Sangwongwanich, G. Angenendt, S. Zurmuhlen, Y. Yang, D. Sera, D. U. Sauer, and F. Blaabjerg, “Enhancing PV inverter reliability with battery system control strategy,” in *CPSS Trans. Power Electron. Appl.*, vol. 3, no. 2, pp. 93–101, Jun. 2018.

[20] M. Sandelic, A. Sangwongwanich, and F. Blaabjerg, "A Systematic Approach for Lifetime Evaluation of PV-Battery Systems," in proc. IECON, 2019, pp. 2295-2300.

[21] S. Stynski, W. Luo, A. Chub, L. G. Franquelo, M. Malinowski, and D. Vinnikov, "Utility-Scale Energy Storage Systems: Converters and Control," in *IEEE Industrial Electronics Magazine*, vol. 14, no. 4, pp. 32-52, Dec. 2020.

[22] C. -T. Tsai, E. M. Ocampo, T. M. Beza and C. -C. Kuo, "Techno-Economic and Sizing Analysis of Battery Energy Storage System for Behind-the-Meter Application," in *IEEE Access*, vol. 8, pp. 203734-203746, 2020.

[23] D. Kucevic et al., “Standard battery energy storage system profiles: Analysis of various applications for stationary energy storage systems using a holistic simulation framework,” in *Journal of Energy Storage*, vol. 28, p. 101077, Apr. 2020, doi: 10.1016/j.est.2019.101077.

[24] Y. Shen, A. Chub, H. Wang, D. Vinnikov, E. Liivik, and F. Blaabjerg, "Wear-Out Failure Analysis of an Impedance-Source PV Microinverter Based on System-Level Electrothermal Modeling," in *IEEE Transactions on Industrial Electronics*, vol. 66, no. 5, pp. 3914-3927, May 2019.

[25] X. Lu, W. Qian, D. Cao, F. Z. Peng, and J. Liu, "A carrier modulation method for minimizing the dc link capacitor current ripple of the HEV DC-DC converter and inverter systems," in proc. *2011 Twenty-Sixth Annual IEEE Applied Power Electronics Conference and Exposition (APEC)*, 2011, pp. 800-807.

[26] Available online: https://www.mouser.ee/datasheet/2/420/United-Chemi-Con-1952507.pdf. Accessed date: 22 June 2021.

[27] “General description of aluminum electrolytic capacitors.” [Online]. Available: http://www.nichicon.co.jp/english/products/pdf/aluminum.pdf

[28] H. Wang, and F. Blaabjerg, “Reliability of capacitors for DC link applications in power electronic converters—an overview,” in *IEEE Trans. Ind. Appl.*, vol. 50, no. 5, pp. 3569-3578, Sep. 2014.

[29] J. Teh, "Uncertainty Analysis of Transmission Line End-of-Life Failure Model for Bulk Electric System Reliability Studies," in *IEEE Transactions on Reliability*, vol. 67, no. 3, pp. 1261-1268, Sept. 2018, doi: 10.1109/TR.2018.2837114.

[30] J. Teh, C. -M. Lai and Y. -H. Cheng, "Impact of the Real-Time Thermal Loading on the Bulk Electric System Reliability," in *IEEE Transactions on Reliability*, vol. 66, no. 4, pp. 1110-1119, Dec. 2017, doi: 10.1109/TR.2017.2740158.

[31] https://www.infineon.com/dgdl/Infineon-AN2019-05_PC_and_TC_Diagrams-ApplicationNotes-v02_01-EN.pdf?fileId=5546d46269e1c019016a594443e4396b

[32] “Military handbook: Reliability prediction of electronic equipment,” Dec. 1991, standard MIL-HDBK-217F.

[33] J. Harms, “Revision of MIL-HDBK-217, reliability prediction of electronic equipment,” pp. 1–3, 2010.

[34] H. Abunima and J. Teh, "Reliability Modeling of PV Systems Based on Time-Varying Failure Rates," in *IEEE Access*, vol. 8, pp. 14367-14376, 2020, doi: 10.1109/ACCESS.2020.2966922.

[35] D.-I. Stroe, M. Swierczynski, A.-I. Stan, R. Teodorescu, and S. J. Andreasen, “Accelerated Lifetime Testing Methodology for Lifetime Estimation of Lithium-Ion Batteries Used in Augmented Wind Power Plants,” in *IEEE Trans. on Ind. Applicat.*, vol. 50, no. 6, pp. 4006–4017, Nov. 2014.

[36] D. Farinet, M. Maurer, L. Vacca, S. V. Spataru, and D.-I. Stroe, "Battery Lifetime Analysis for Residential PV-Battery System used to Optimize the Self Consumption - A Danish Scenario," in proc. 2019 IEEE Energy Conversion Congress and Exposition (ECCE), Sep. 2019.

[37] Daniel-Ioan Stroe, "Lifetime models for lithium-ion batteries used in virtual power plant applications," Ph.D. Thesis AAU, 2014.

[38] Adam Nieslony (2021). Rainflow Counting Algorithm (https://www.mathworks.com/matlabcentral/fileexchange/3026-rainflow-counting-algorithm), MATLAB Central File Exchange. Retrieved July 3, 2021.

[39] N. Andrenacci, E. Chiodo, D. Lauria, and F. Mottola, "Life Cycle Estimation of Battery Energy Storage Systems for Primary Frequency Regulation," in *Energies*, vol. 11, no. 12, p. 3320, Nov. 2018, doi: 10.3390/en11123320.